Microsolvation of Alkali and Halide Ions in Acetonitrile Clusters

Tao-Nhân V. Nguyen and Gilles H. Peslherbe*

Centre for Research in Molecular Modeling and Department of Chemistry & Biochemistry, Concordia University, Montréal, Québec, Canada, H3G 1M8

Received: March 15, 2002; In Final Form: August 21, 2002

The room-temperature thermodynamic and structural properties of acetonitrile clusters containing alkali ions (Na^+, Cs^+) or halide ions (I^-) are investigated via Monte Carlo simulations. An intermolecular potential function including Coulombic, polarization, and repulsion−dispersion terms was parameterized on the basis of high-level CCSD(T)/6-311+G(2df,pd)//MP2/6-311+G(d) ab initio calculations, supplemented by experimental data for molecular and ionic polarizabilities. Cluster thermodynamic properties such as binding enthalpies evaluated from the Monte Carlo simulations are in good agreement with available experimental data, which inspires confidence in the simulation results. These properties are shown to converge very slowly to their bulk limit, in agreement with earlier predictions of the liquid drop model, and their evolution with cluster size is closely related to the solvation structure of the ionic clusters. All $Na^+(CH_3CN)_n$, $Cs^+(CH_3CN)_n$, and $I^-(CH_3CN)_n$ clusters exhibit an interior solvation structure. However, if the $Na^+(CH_3CN)_n$ and $Cs^+(CH_3CN)_n$ room-temperature radial probability distributions exhibit very distinct, sharp peaks, those for large $I^-(CH_3CN)_n$ clusters are broader, because of much weaker iodide−solvent interactions. The solvent coordination numbers for the first solvation shell are ca. 6, 7, and 9 for $Na^+(CH_3CN)_n$, $Cs^+(CH_3CN)_n$ and $I^-(CH_3CN)_n$ clusters, respectively. The completion of the ion first solvation shell is accompanied by a significant decrease of the stepwise binding enthalpies, a finding that is more pronounced for cationic clusters. Finally, comparison with previous results for ion−water clusters demonstrated the importance of the relative strengths of ion−solvent and solvent−solvent interactions in the determination of interior vs surface ionic cluster structures. For example, $I^-(CH_3CN)_n$ clusters clearly exhibit an interior solvation structure, in net contrast with the surface structures observed for $I^-(H_2O)_n$ clusters.

I. Introduction

Because a large fraction of chemical reactions occur in solution, considerable attention has been paid to the influence of solvent on the physical and chemical properties of species.[1−5] By that token, experimental and theoretical studies of clusters−an intermediate state of the matter between the condensed and gas phases−are very valuable for gaining insight into such fundamental processes as the role of microsolvation in chemical reactions.[6−10] Over the past decade, an increasing number of cluster types have been investigated,[11] due to the development of experimental techniques for generating such species and observing their properties.[12] For example, studies of simple ionic clusters have provided detailed information about the cluster structures, thermodynamics, and spectroscopic properties.[13−19] Of particular interest is the investigation of the properties of clusters of increasing size in order to determine at which point cluster properties would converge to bulk phase values.[20,21] A number of experimental and theoretical studies have been reported about the solvation of ion pairs in clusters.[20−34] Salt ion pairs such as NaI in polar solvent clusters are of particular interest to us. The NaI system has been a prototype system for the study of photodissociation dynamics involving curve crossing of covalent and ionic states.[35−37] Briefly, NaI photoexcitation results in transient trapping in an excited-state well that arises from the avoided crossing between ionic and covalent states, together with a decay of the excited-state population into atomic products via nonadiabatic transitions.[38,39] In typical femtosecond pump−probe experiments, the excited-state population can be time-resolved by ionization of the trapped excited NaI to a probe state and collection of the dissociation products with a mass spectrometer.[27,39] Our early theoretical work on $NaI(H_2O)$ clusters[40] showed how the presence of solvent affects the nonadiabatic dynamics of the photodissociation process and prompted experimental studies of NaI ion pairs in polar solvent clusters of water, acetonitrile, and ammonia.[27−29] In these experiments, a very clear solvent-selective behavior was observed in the distribution of the detected $Na^+(solvent)_n$ product ions.[27] For instance, clusters of size up to $n \sim 50$ have been observed experimentally with water, but no clusters larger than size 10 and 7 have been observed with ammonia and acetonitrile, respectively.

In previous theoretical work, we also investigated the structure and thermodynamics of NaI ion pairs in aqueous clusters.[25,26] We found that NaI ion pairs are actually stable with respect to complete ground-state dissociation, even in very large water clusters, but that solvent-separated ion pairs become rapidly predominant over contact ion pairs with increasing cluster size. Model electronic structure calculations showed that solvent-separated ion pairs have a much reduced oscillator strength and may not possess optically accessible excited states akin to that of gas-phase NaI.[26] Our findings are consistent with the fact that products of $NaI(H_2O)_n$ cluster photodissociation of size $n > 50$ were not observed experimentally, as the larger solvent-separated ion-pair parent clusters may just not be photochemically active. Interestingly enough, we also found that the structure of ion pairs in water clusters could be relatively simply related to that of the individual ions in water clusters.[25] Of

10.1021/jp020728x CCC: $25.00 © 2003 American Chemical Society
Published on Web 02/15/2003

particular importance in this case is the now well-known "hydrophobic" character of the iodide ion in aqueous clusters,[18,41] which may explain why NaI ion pairs are "dragged" to the surface of small water clusters.[25]

We are now turning our attention to acetonitrile and ammonia clusters in order to understand the experimental differences observed for the various solvents.[27] The first step involves the development and validation of model potentials for Monte Carlo simulations of the structure and thermodynamics of NaI ion pairs in clusters. While we defer our work on ammonia clusters to a separate publication,[42] in this work, we derive model potentials for simulations of acetonitrile clusters and validate the potentials by comparing the results of ionic cluster simulations with available experimental thermochemical data. Model potentials for acetonitrile simulations have been proposed in previous work,[14,43−46] but none of them seemed to be completely adequate for our cluster simulations. We naturally focus on $Na^+(CH_3CN)_n$ and $I^-(CH_3CN)_n$ clusters, but also investigate $Cs^+(CH_3CN)_n$ clusters for comparison. The Cs^+ ion is a monovalent cation like Na^+ but of a size similar to that of I^-, and this may help untangle the role of ion size and charge in determining the structure of ionic clusters. The photodissociation of CsI in solvent clusters is also being investigated experimentally,[47] and theoretical studies akin to our previous work[26,40] on NaI in water clusters might be needed for that system. Finally, a key point of this work is to compare the structural properties of ion−acetonitrile clusters to those of aqueous clusters.[25,48] Despite both being highly polar solvents, acetonitrile and water differ significantly due to very different molecular sizes and dipole moments and the propensity of water to form relatively strong hydrogen bonds. Because the latter plays a major role in determining the surface structure of $I^-(H_2O)_n$ clusters, we will pay particular attention to the structure of $I^-(CH_3CN)_n$ clusters.

The outline of this article is as follows. The simulation procedure is briefly presented in section II. The thermodynamic and structural properties of the ion−acetonitrile clusters resulting from the simulations are presented and discussed in section III, where they are compared and contrasted to previous findings for ion−water clusters. Concluding remarks follow in section IV.

II. Computational Procedure

A. Monte Carlo Simulations. Metropolis Monte Carlo simulations[49] are used to investigate the thermodynamic and structural properties of $Na^+(CH_3CN)_n$, $Cs^+(CH_3CN)_n$, and $I^-(CH_3CN)_n$ clusters at 300 K. We follow the procedure developed in previous work,[25] where independent simulations are carried out for clusters of various sizes. A given number n of CH_3CN molecules is placed around a fixed ion, and canonical ensembles are generated as Markov chains of cluster configurations.[50] We employ the random-walk method[34] to generate a new trial solvent configuration by randomly translating one acetonitrile molecule in each Cartesian direction and rotating it about its standard Euler angles θ, ψ, and φ.[51] Since each random walk involves the six degrees of freedom of only one acetonitrile molecule, the length of the Markov chain is naturally increased with cluster size. Only sampled configurations for which all acetonitrile molecules have changed position are stored for structural analysis. Finally, the clusters are periodically heated and cooled with a smooth temperature schedule in order to attempt sampling all possible local minima.[52]

In contrast to liquid simulations,[51] no potential truncation is necessary and no periodic boundary conditions are imposed in cluster simulations. However, complications arise from the fact that acetonitrile molecules may undergo evaporation at room temperature,[53] which results in a reduction of the size of the cluster being simulated.[54] Since our goal is to obtain a well-defined equilibrium ensemble of clusters of a given size, each Markov chain containing clusters that have undergone solvent evaporation is excluded from the final conformational sampling (in practice, acetonitrile is considered as evaporated from the cluster when it is further than 20 Å from the ion). This is formally equivalent to adding a step-function to the configurational integral, so as not to take into account clusters that are not of the appropriate size.[55,56] Each run entails about 10^6 steps of equilibration, followed by an equivalent number of steps for data collection. The range of displacement for translational and rotational motion was chosen so as to obtain acceptance ratios between 40 and 60%. This typically corresponds to a displacement range of 0.25 Å for translation and 25°, 0.25, and 25° for φ, cos θ, and ψ, respectively.

Cluster enthalpies are computed from the average energies $\langle V \rangle$ of the canonical ensembles of configurations as

$$\Delta H_n = \Delta U + \Delta(PV) = \langle V \rangle + nRT \tag{1}$$

where n is the number of solvent molecules in the cluster[57] and stepwise binding enthalpies are simply obtained as

$$\Delta H_{n,n-1} = \Delta H_{n-1} - \Delta H_n \tag{2}$$

Structural properties of the clusters are analyzed in terms of a distance-dependent coordination number $N_{coord}(r)$, and its derivative, which is the normalized radial probability distribution function

$$P(r) = \frac{dN_{coord}(r)}{dr} = n\frac{4\pi r^2 g(r)}{\int_0^\infty 4\pi r^2 g(r)\, dr} \tag{3}$$

It should be noted that $P(r)$ differs from the radial distribution functions $g(r)$ used in liquid structure theory[51] by a factor $4\pi r^2$, and it actually represents spatial relative probabilities. The probabilities are normalized so that integral distributions equal the number of solvent molecules present in the cluster.

B. Model Potentials. Early model potentials for acetonitrile did not explicitly include hydrogen atoms[43,44] or they employed a very simple empirical potential function.[45] We tested a more recently proposed potential,[14] which includes Coulombic, distributed polarizability, and repulsion−dispersion terms, but the model seems to underestimate solvent polarization effects in the presence of ions.[58] Another model was parameterized for pure acetonitrile[46] and sodium−acetonitrile[59] liquid simulations, based on ab initio calculations that do not take into account zero-point energy corrections for the acetonitrile−acetonitrile binding energy. Further, the sodium−acetonitrile polarization interactions were added to the potential function in an ad hoc fashion.[59] Hence, we have opted to develop a new model potential function describing both solvent−solvent interactions and ion−solvent interactions for simulating alkali and halide ions in acetonitrile clusters.

In our simulations we employ rigid acetonitrile molecules, and the interaction energy between various monomers (including the ion) consists of Coulombic, many-body polarization, and repulsion−dispersion contributions,

$$V = V_{Coul} + V_{pol} + V_{rep-disp} \tag{4}$$

The Coulombic part,

$$V_{\mathrm{Coul}} = \sum_i \sum_j \frac{q_i \cdot q_j}{|\mathbf{r}_i - \mathbf{r}_j|} \tag{5}$$

simply represents the interactions between the fractional charges q_i on each atomic site (at position r_i) of the monomers. The ion and each acetonitrile molecule carry an isotropic polarizable site (that is located on the middle carbon for CH_3CN) with a polarizability α_i and an induced dipole moment $\boldsymbol{\mu}_i$. The polarization contribution is expressed as[60]

$$V_{\mathrm{pol}} = -\frac{1}{2}\sum_i \mathbf{E}_i^{\mathrm{o}} \boldsymbol{\mu}_i \tag{6}$$

where the electric field $\mathbf{E}_i^{\mathrm{o}}$ due to the permanent charges of the other monomers is given by

$$\mathbf{E}_i^{\mathrm{o}} = \frac{\sum_j q_j \mathbf{r}_j}{|\mathbf{r}_i - \mathbf{r}_j|^3} \tag{7}$$

and the induced dipole moments are calculated from

$$\boldsymbol{\mu}_i = \alpha_i \mathbf{E}_i = \alpha_i[\mathbf{E}_i^{\mathrm{o}} + \sum_{j \neq i} T_{ij} \boldsymbol{\mu}_j] \tag{8}$$

in a self-consistent iterative procedure. T_{ij} in eq 8 is the dipole tensor.[60] The polarizable sites included in the induced dipole problem of eqs 6−8 account for mutual polarization of the solvent molecules and the solute ion. In cluster simulations, the low dimensionality of the problem allows one to solve the set of linear equations in eq 8 in matrix form.[61] In the present work, the induced dipoles are solved by LU decomposition and back-substitution.[50] Finally, short-range repulsion and dispersion interactions are modeled via Lennard-Jones potentials with well depth ϵ_{ij} and size parameter σ_{ij} between all atoms.

$$V_{\mathrm{rep-disp}} = \sum_{i,j} 4\epsilon_{ij}\left[\left(\frac{\sigma_{ij}}{r_{ij}}\right)^{12} - \left(\frac{\sigma_{ij}}{r_{ij}}\right)^{6}\right] \tag{9}$$

First-principles quantum chemistry calculations provide the basis for the parameterization of our model potentials. Accordingly, we now turn our attention to ab initio calculations for small clusters.

C. Ab Initio Calculations. Ground-state properties of $(CH_3CN)_{1-2}$, $Na^+(CH_3CN)_{1-4}$, $Cs^+(CH_3CN)_{1-3}$, and $I^-(CH_3CN)_{1-2}$ clusters were calculated with the quantum chemistry packages GAMESS[62] and Gaussian 98.[63] Cluster structures were first optimized with acetonitrile molecules constrained to the isolated molecule geometry. The intramolecular coordinates were subsequently allowed to relax before a frequency calculation was performed in order to characterize the stationary points and obtain harmonic zero-point energies. This procedure allows us to estimate the energy gain associated with monomer geometry relaxation in clusters, and to estimate the extent of the error introduced in our model potential by employing rigid solvent molecules. A number of model chemistries were tested, including Hartree−Fock (HF),[64] second-order Møller−Plesset (MP2),[64] and Becke 3 Lee−Yang−Parr (B3LYP) theories,[65,66] together with standard 6-31G(d) and 6-311+G(d) basis sets.[64] Stuttgart-Dresden-Bonn quasi-relativistic effective core potentials (ECP) and valence basis sets[67] with additional polarization functions were employed for the I^- and Cs^+ ions, and an all-electron 6-311+G(d) basis set recently reported for iodine was also used for comparison.[68] As will become evident in the following, we found that, overall, the MP2/6-311+G(d) model chemistry is quite reliable, with the advantage of being computationally feasible for larger clusters. Energetics of the smaller clusters were also evaluated at the coupled cluster with single, double, and linearized triple excitation [CCSD(T)] level of theory with a 6-311+G(2df,pd) basis set,[69] using the MP2/6-311+G(d) cluster geometries.

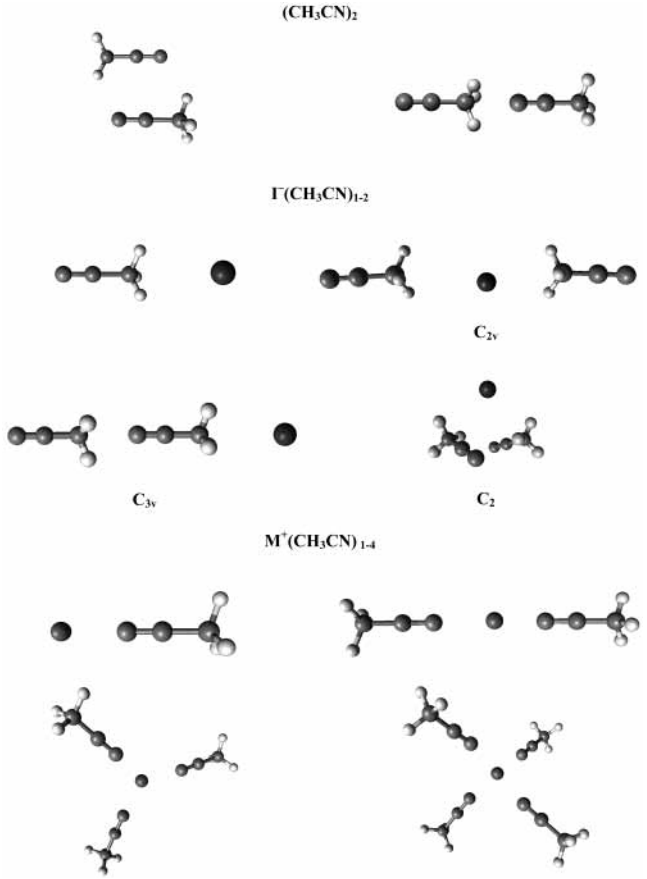

Figure 1. Minimum energy structures of $(CH_3CN)_2$, $M^+(CH_3CN)_{1-4}$ [M = Cs,Na], and $I^-(CH_3CN)_{1-2}$ clusters predicted by the MP2/6-311+G(d) model chemistry.

The cluster minimum energy structures obtained from ab initio calculations are shown in Figure 1, and the results of the calculations are collected in Table 1 for a number of small clusters. The MP2/6-311+G(d) model chemistry reproduces the experimental CH_3CN geometry, which is essentially the same in the liquid phase[70] and in the gas phase,[71] and the computed dipole moment compares very well to its experimental counterpart of 3.92 D.[72] This inspires confidence in this level of ab initio quantum chemistry. We are reporting geometric parameters in Table 1 for the clusters after monomer geometry relaxation to illustrate the effect of constraining monomer geometries to their experimental values. The latter is obviously not significant. In general, the C−H bonds are shortened by only 0.01 Å, relative to the isolated acetonitrile molecule, and the C−N bond lengthens in $I^-(CH_3CN)_n$ clusters by only 0.01 Å. Properties such as binding energies or charge distributions are actually not affected by monomer geometry constraints. The molecular dipole moments of individual monomers can be evaluated from the ESP charge distribution[73] of the supermolecule, and they are also listed in Table 1.

TABLE 1: Properties of Small Pure Solvent and Ionic Clusters[a]

geometric parameters						$D_e^{n,n-1}$ [b] (no BSSE)	$D_0^{n,n-1}$ [b] (no BSSE)	$D_0^{n,n-1}$ [b]	$\Delta H_{n,n-1}$ [c]	μ_{CH_3CN} [d]
				$(CH_3CN)_n$						
	R_{C-CM} [e]	R_{CM-H}	R_{C-N}	R_{C-C} [f]	R_{N-H} [g]					
(CH_3CN)	1.46	1.10	1.17							3.9
$(CH_3CN)_2$ C_{2h}	1.46	1.09	1.17	3.35	2.55	6.4 (6.0)	5.7 (5.3)	4.3 (4.7)		4.2, 4.2
$(CH_3CN)_2$ C_{3v}	1.46	1.09	1.17			3.0 (3.2)	2.8 (2.9)	2.2 (2.5)		4.3, 4.0
				$Na^+(CH_3CN)_n$						
	R_{C-CM}	R_{CM-H}	R_{C-N}	R_{Na-N}						
$Na^+(CH_3CN)$	1.46	1.09	1.17	2.31		30.7 (31.1)	30.0 (30.4)	29.3 (29.5)		5.4
$Na^+(CH_3CN)_2$	1.46	1.09	1.17	2.34		26.7	26.1	25.1	24.4 ± 0.3 [h]	4.9
$Na^+(CH_3CN)_3$	1.46	1.09	1.17	2.38		20.3	19.8	19.1	20.6 ± 0.5	4.8
$Na^+(CH_3CN)_4$	1.46	1.09	1.17	2.41		16.2	15.5	14.2	14.9 ± 0.2	4.7
				$Cs^+(CH_3CN)_n$ [ECP]						
	R_{C-CM}	R_{CM-H}	R_{C-N}	R_{Cs-N}						
$Cs^+(CH_3CN)$	1.46	1.09	1.17	3.17		17.4 (19.2)	17.0 (18.8)	16.5 (18.1)	19.2 ± 0.1 [i]	4.7
$Cs^+(CH_3CN)_2$	1.46	1.09	1.17	3.22		15.5	15.2	13.0	16.7 ± 0.1	4.7
$Cs^+(CH_3CN)_3$	1.46	1.09	1.17	3.22		13.5	13.4	12.7	14.3 ± 0.1	4.6
				$I^-(CH_3CN)_n$						
	R_{C-CM}	R_{CM-H}	R_{C-N}	R_{CM-I}						
$I^-(CH_3CN)$	1.46	1.09	1.18	3.70		11.5 (10.9)	11.4 (10.9)	9.9 (10.5)	11.0 ± 0.2 [j]	5.0
$I^-(CH_3CN)_2$ C_{3v}	1.46	1.09	1.18	3.65, 9.43		6.2	6.2	5.4		5.0, 5.0
$I^-(CH_3CN)_2$ C_2	1.46	1.09	1.18	3.95		11.1	10.1	7.2	10.4 ± 0.2 [j]	5.0
$I^-(CH_3CN)_2$ C_{2v}	1.46	1.09	1.18	3.95		10.0	9.8	9.0		4.7
				$I^-(CH_3CN)_n$ [ECP]						
	R_{C-CM}	R_{CM-H}	R_{C-N}	R_{CM-I}						
$I^-(CH_3CN)$	1.46	1.09	1.18	3.76		12.4 (11.1)	12.0 (10.6)	8.4 (10.1)	11.0 ± 0.2 [j]	5.7
$I^-(CH_3CN)_2$ C_{3v}	1.46	1.09	1.18	3.71, 9.50		6.5	6.1	5.2		4.6, 4.4
$I^-(CH_3CN)_2$ C_2	1.46	1.09	1.18	3.94		9.9	8.9	6.2	10.4 ± 0.2 [j]	5.2
$I^-(CH_3CN)_2$ C_{2v}	1.46	1.09	1.18	3.82		9.3	9.0	8.5		4.9

[a] All properties are calculated with the MP2/6-311+G(d) model chemistry, except for the numbers in parentheses, which are CCSD(T)/6-311+G(2df,pd)//MP2/6-311+G(d) values. SDD effective core potentials (ECP) are used as indicated; all other results are obtained from all-electron calculations. Internuclear distances are in angstroms (Å) and binding energies in kcal/mol. [b] Stepwise binding energies for clusters of size *n*. D_e is the classical binding energy while D_0 is the zero-point energy-corrected binding energy. Values are corrected for BSSE unless indicated otherwise. [c] Experimental stepwise binding enthalpy in kcal/mol. [d] Dipole moment of acetonitrile molecule(s) in Debye (D), calculated from ESP charge distributions. [e] C_M is the methyl carbon. [f] Distance between the central carbons of the acetonitrile molecules. [g] Distance between the nitrogen atom of a molecule and the hydrogen in the symmetry plane of the other molecule. [h] Taken from ref 95. [i] Taken from ref 80. [j] Taken from ref 96.

Binding energies (D_0) are calculated via the supermolecule approach, including zero-point energy corrections and a correction for basis set superposition error (BSSE) estimated with the counterpoise method.[74] The zero-point energy correction is based on the MP2/6-311+G(d) harmonic frequencies. Monomer relaxation in the counterpoise calculations is not an issue here, because we constrain the acetonitrile molecules to the isolated molecule geometries in all calculations but for frequencies. Also, because the counterpoise method tends to overestimate the BSSE,[75,76] we report binding energies with and without BSSE corrections. It is obvious from Table 1 that the zero-point energy and BSSE corrections to the binding energy amount to at most 2 kcal/mol for all clusters considered, except for $I^-(CH_3CN)_n$ clusters. Experimental binding enthalpies are listed in Table 1 for comparison and perspective; they may be good estimates of the binding energies, if enthalpies are not strongly temperature-dependent (assuming a rare gas relationship, stepwise room-temperature binding enthalpies might only differ from binding energies by $RT = 0.6$ kcal/mol).

Previous calculations[77,78] of the potential energy surface for $(CH_3CN)_2$ have demonstrated the existence of two stable isomers for pure acetonitrile dimers (shown in Figure 1), one with antiparallel dipoles, and the other with linear head-to-tail dipoles, a finding that is supported by experimental evidence.[79] The binding energy of the linear local minimum (1.8 kcal/mol) was reported to be about half of that for the antiparallel dimer configuration (3.7 kcal/mol).[77] Our MP2/6-311+G(d) calculations are consistent with these findings. The linear local minimum has C_{3v} symmetry, with the hydrogen atoms in an eclipsed configuration; the molecules are separated by a distance $r_{N-C} = 3.26$ Å, and the presence of the nitrogen atom in the vicinity of the other acetonitrile molecule slightly increases that molecule's $C-C_M-H$ bending angle (by 0.5°) in the relaxed structure. The antiparallel configuration has C_{2h} symmetry, with the molecular axes in the σ_h symmetry plane and the hydrogen atoms in this plane pointing toward the nitrogen atom of the other molecule, and the central carbons are separated by 3.35 Å, which incidentally corresponds to the interchain spacing reported in the liquid phase.[80] Because of a slight bending of the C_M-C-N axis (179.3°) in the relaxed structure, the monomers lose their C_{3v} symmetry, but the energy gained by allowing this slight deformation is only 0.2 kcal/mol. The binding energies obtained in this work for both dimer structures are in good qualitative agreement with those previously reported,[77] but our calculations predict slightly larger binding energies, i.e., 2.2 kcal/mol for the C_{3v} linear dimer and 4.3 kcal/mol for the C_{2h} antiparallel configuration with MP2/6-311+G(d). Higher-level CCSD(T)/6-311+G(2df,pd)//MP2/6-311+G(d)

calculations also support larger binding energies for the acetonitrile dimers. Finally, we note that the mutual polarization of the acetonitrile molecules in the dimer is not negligible and increases the dipole moments of the acetonitrile molecules by ~10%.

Previous ab initio calculations at the HF level with a double-ζ-quality valence basis set[15] predicted stable high-symmetry structures for $Na^+(CH_3CN)_n$ clusters, with the ion aligned in the acetonitrile molecular axis (on the nitrogen side). The structures obtained in the present work for small $Na^+(CH_3CN)_n$ clusters are in good agreement with this finding, and the cluster structures (shown in Figure 1) are found to be linear, trigonal planar, and tetrahedral for $n = 2$, 3, and 4, respectively. The sodium ion is found to lie between 2.3 and 2.4 Å from the acetonitrile nitrogen, with a separation increasing with cluster size. This distance is slightly larger than the separation observed in previous work,[15,81] which arises from inclusion of electronic correlation in our calculations. For cluster sizes 2 to 4, the MP2/6-311+G(d) binding energies are within ca. 1 kcal/mol of the available experimental binding enthalpies. This is quite an improvement over previous results,[15] which deviated from experimental values by 5 kcal/mol, again because of the lack of electronic correlation. Finally, we note that increasing the size of the basis set and using a higher level of theory only improve the binding energy of $Na^+(CH_3CN)$ by 0.2 kcal/mol.

To our knowledge, no prior calculations have been reported for cesium−acetonitrile complexes. The minimum energy structures of $Cs^+(CH_3CN)_n$ clusters are similar to those obtained for sodium clusters. It should be noted that the $Cs^+(CH_3CN)_2$ minimum energy structure is found to be linear, and not slightly bent like that of $Cs^+(H_2O)_2$.[82] The ion−nitrogen distance increases from 2.34 Å in $Na^+(CH_3CN)_n$ to 3.17 Å in $Cs^+(CH_3CN)_n$ clusters. Structural similarities can be attributed to the fact that both Cs^+ and Na^+ are monovalent cations, giving rise to similar electrostatic interactions with acetonitrile molecules, and not surprisingly, electrostatic interactions seem to govern the determination of the cluster structure. However, because of the larger size and more diffuse positive charge of Cs^+, the ion−molecule interactions are weaker. This results not only in larger ion−molecule equilibrium distances but also in smaller binding energies for $Cs^+(CH_3CN)_n$ clusters relative to those for $Na^+(CH_3CN)_n$. For instance, the CCSD(T)/6-311+G(2df,pd)//MP2/6-311+G(d) binding energy is 29.5 kcal/mol for $Na^+(CH_3CN)$, while it is only 18.1 kcal/mol for $Cs^+(CH_3CN)$. If the latter number is in good agreement with the experimental $Cs^+(CH_3CN)$ binding enthalpy, in general the MP2/6-311+G(d) binding energies seem to deviate from experimental binding enthalpies significantly more for $Cs^+(CH_3CN)_n$ clusters than for $Na^+(CH_3CN)_n$. This could be due to a poorer description of the ion−solvent interactions due to the ECP treatment of the cesium ion.

We now turn our attention to small iodide−acetonitrile complexes. The optimized geometry of the $I^-(CH_3CN)$ cluster has the ion in the C_{3v} axis, but obviously on the methyl side of acetonitrile.[83] The strong electrostatic attraction between the hydrogen atoms of acetonitrile and the ion causes a slight distortion of the $C-C_M-H$ angle (by 1°) in the relaxed $I^-(CH_3CN)$ structure. The all-electron MP2/6-311+G(d) binding energies for $I^-(CH_3CN)$, with and without BBSE correction, bracket the experimental number for the cluster binding enthalpy, and high-level CSSD(T) calculations seem to perform remarkably well. The binding energies obtained with ECPs, with and without BSSE correction, also bracket the experimental number, but they deviate from the latter more significantly. Despite the similar size of the ions, the binding energy of $I^-(CH_3CN)$ is less than that of $Cs^+(CH_3CN)$, because of the weaker interaction of acetonitrile with negative ions. The latter is due to the diffuse distribution of the positive pole of the dipole over the H atoms of the molecule, while interactions with cations via the charge-concentrated negative nitrogen are much stronger.

As for $I^-(CH_3CN)_2$, three isomers that lie close in energy were identified.[84] According to the MP2/6-311+G(d) calculations reported here, the most stable structure has a C_{2v} quasi-linear configuration ($\alpha_{CM-I-CM} = 168°$), with the methyl groups in eclipsed configuration. The second isomer corresponds to a C_{3v} structure, higher in energy by 3 to 4 kcal/mol, with the acetonitrile molecules aligned on one side of the ion and the iodide ion along the acetonitrile molecular axis. The last isomer has C_2 symmetry, with the acetonitrile molecules oriented in a perpendicular fashion, and results from a combination of hydrogen bonding of acetonitrile to the ion and ion−dipole interactions.[84] The latter isomer has a calculated binding energy comparable to that of the C_{2v} isomer, especially before inclusion of the approximate BSSE correction. We note that the results are obviously very sensitive to the choice of model chemistry and the treatment of BSSE, and a more comprehensive study of the actual nature of the $I^-(CH_3CN)_2$ structure is deferred to another publication.[85] We also note that previous studies[19] of $Br^-(CH_3CN)_n$ clusters employing density functional theory showed comparable results but with some additional structures involving hydrogen bonding. A full discussion of halide−acetonitrile clusters and the sensitivity of the results to the model chemistry employed will also be given somewhere else.[86]

Finally, the magnitude of the ESP charge of the ions in the ionic clusters (not listed) is ca. ± 0.98e, which demonstrates very little electron transfer between the ion and the solvent molecules. This provides support for a model potential primarily based on electrostatics and employing unit point charges for the ions. We note from the molecular dipole moments listed in Table 1 that the CH_3CN polarity increases significantly from its gas-phase value when placed in the vicinity of another solvent molecule or an ion. For example, the acetonitrile dipole moment increases by 0.3 D in the presence of another solvent molecule and by 1.0 to 1.5 D in the presence of an ion.

D. Parametrization of Model Potentials. The parameters for our model potential include point charges (q_i), polarizabilities (α_i), and Lennard-Jones terms (ϵ_{ij}, σ_{ij}). All parameters are derived on the basis of ab initio data, with the exception of polarizabilities, and are listed in Table 2. As discussed in the previous section, the ab initio data were obtained for pure-solvent and ionic clusters where the acetonitrile molecule is typically constrained to the isolated molecule geometry, since our model potential employs rigid solvent molecules with that geometry. We did ensure that monomer geometry relaxation had very little impact on the ab initio predictions of such properties as cluster geometries, binding energies, and electric properties. The fractional atomic charges for acetonitrile are assigned on the basis of the MP2/6-311+G(d) ESP charge distribution, which is obtained by fitting the electrostatic potential over a large grid of points,[87] while the ions simply carry a positive or negative unit charge. Polarizabilities are notoriously difficult to determine accurately with quantum chemistry, and thus the polarizabilities associated with the ionic and molecular polarizable sites are taken from gas-phase experimental data.[88,89] Finally, the Lennard-Jones parameters (σ_{ij},ϵ_{ij}) are adjusted[90] to fit the $(CH_3CN)_2$, the $Na^+(CH_3CN)_{1-2}$, the $Cs^+(CH_3CN)_{1-2}$, and the $I^-(CH_3CN)_{1-2}$ calculated geom-

TABLE 2: Model Potential Parameters[a]

atomic point charges

	N	C	C_M	H	Na	I	Cs
q_i	−0.49	0.48	−0.56	0.19	1.00	−1.00	1.00

molecular and ionic polarizabilities

	CH_3CN	Na^+	I−	Cs^+
α_I	4.5	0.2	5.3	3.1

solvent−solvent Lennard-Jones parameters

	N−N	C−N	H−N	C−C	H−C	H−H
ϵ_{ij}	50	30	50	3	40	40
σ_{ij}	3.50	3.60	2.70	3.80	2.80	1.90

ion−solvent Lennard-Jones parameters

	Na^+−N	Na^+−C	Na^+−H	Cs^+−N	Cs^+−C	Cs^+−H	I^--N	I^--C	I^--H
ϵ_{ij}	50	500	50	800	750	700	40	857	34
σ_{ij}	3.00	3.40	2.30	3.20	4.30	3.30	4.52	3.20	3.95

[a] Point charges (q_i) in fractions of e, polarizabilities (α_i) in Å^3, Lennard-Jones parameters ϵ_{ij} in cal/mol and σ_{ij} in Å.

TABLE 3: Properties of Small Clusters Predicted by the Model Potential[a]

	R_{C-C}	R_{N-H}[b]	$R_{cation-N}$	R_{I-CM}	$D_0^{n,n-1}$[c]	μ_{CH_3CN}[d]
$(CH_3CN)_2$	3.35	2.57			4.7	4.3
			$Na^+(CH_3CN)_n$			
$Na^+(CH_3CN)$			2.30		29.3	5.6
$Na^+(CH_3CN)_2$			2.33		25.9	5.4
$Na^+(CH_3CN)_3$			2.35		20.7	5.2
$Na^+(CH_3CN)_4$			2.38		16.2	4.9
			$Cs^+(CH_3CN)_n$			
$Cs^+(CH_3CN)$			3.15		18.6	5.1
$Cs^+(CH_3CN)_2$			3.17		16.4	4.9
$Cs^+(CH_3CN)_3$			3.19		14.4	4.8
			$I^-(CH_3CN)_n$			
$I^-(CH_3CN)$				3.68	10.5	4.7
$I^-(CH_3CN)_2$ C_{3v}				3.65/8.83	5.3	4.9/4.3
$I^-(CH_3CN)_2$ C_2				3.61	8.6	4.7
$I^-(CH_3CN)_2$ C_{2v}				3.73	9.7	4.6

[a] Internuclear distances in Å. [b] Distance between the nitrogen atom of a molecule and the hydrogen in the symmetry plane of the other molecule in Å. [c] Stepwise binding energy in kcal/mol. [d] Molecular dipole moment of acetonitrile in D.

etries and binding energies.[91] Attention is also paid to the dipole moments of acetonitrile in clusters, which primarily depend on the cluster geometry. The fitting procedure was performed with a nonlinear least squares program based on the Marquardt−Levenberg algorithm.[50]

Inspection of Table 3 shows that structural properties for $(CH_3CN)_2$, $Na^+(CH_3CN)_{1-4}$, $Cs^+(CH_3CN)_{1-3}$, and $I^-(CH_3CN)$ determined with our model potentials agree well with their ab initio counterparts. For instance, bond lengths are reproduced within 3% for all clusters. This is an indication of the reliability of the model potential for reproducing cluster geometries. Not surprisingly, energetic properties such as stepwise binding energies are less accurately reproduced with simple model potentials, when compared to the ab initio data, and the difference between the two increases with cluster size. However, the model binding energies are still within ∼2 kcal/mol of the quantum chemistry values, which may be the error bar that one can assign to the ab initio results in the first place. Finally, the CH_3CN dipole moments seem to be reproduced almost quantitatively with the simple induction model of our potential. This model is, to our knowledge, the first one to successfully reproduce a significant increase of the CH_3CN polarity from its gas-phase value when placed in the vicinity of another solvent molecule or an ion, as discussed earlier. For example, the acetonitrile dipole moment increases by 0.4 D in the presence of another solvent molecule and by 1.0 to 1.7 D in the presence of an ion.

TABLE 4: Stepwise Binding Enthalpies $\Delta H_{n,n-1}$

	$Na^+(CH_3CN)_n$		$Cs^+(CH_3CN)_n$		$I^-(CH_3CN)_n$	
n	calcd.[a]	expt.[b]	calcd.[a]	expt.[c]	calcd.[a]	expt.[d]
1	28.8		19.1	19.2	9.8	11.0
2	25.2	24.4	16.9	16.7	8.9	10.4
3	20.1	20.6	14.7	14.3	7.7	9.2
4	15.3	14.9	12.4	12.1	6.5	7.8
5	11.4	12.7	9.6	10.9	6.2	7.1

[a] Stepwise binding enthalpies obtained from room-temperature Monte Carlo simulations. [b] Taken from ref 96. [c] Taken from ref 81. [d] Taken from ref 97.

III. Results and Discussion

A. Thermodynamic Properties. The stepwise binding enthalpies obtained from room-temperature Monte Carlo simulations are listed in Table 4. Comparison with the experimental stepwise binding enthalpies for small clusters suggests that our model potentials are adequate for describing many-body interactions in the larger clusters. The largest deviations of the stepwise binding enthalpy are 1.3, 1.3, and 0.9 kcal/mol for $Na^+(CH_3CN)_n$, $Cs^+(CH_3CN)_n$, and $I^-(CH_3CN)_n$ clusters, respectively. To our knowledge, the $Na^+(CH_3CN)$ binding enthalpy has not been measured experimentally, and the results of our simulations suggest that we can predict this number to be 29 kcal/mol with some degree of confidence.

The calculated binding enthalpies are displayed as a function of cluster size in Figure 2. One might expect the stepwise binding enthalpy to reach a plateau converging to the liquid-phase enthalpy of vaporization. This can be illustrated in the top panel of Figure 2, where the reduced binding enthalpies, i.e., the binding enthalpies per solvent molecule $\Delta H_n/n$, are shown as a function of cluster size n. The reduced binding enthalpy is closely related to the average amount of heat necessary to vaporize one acetonitrile molecule from the cluster. We note that all curves seem to converge to the liquid-phase acetonitrile heat of vaporization, $\Delta H_{vap} = 7.9$ kcal/mol.[92] For example, the deviations observed are respectively 2.0, 1.7, and 2.7 kcal/mol for $Na^+(CH_3CN)_{36}$, $Cs^+(CH_3CN)_{36}$, and

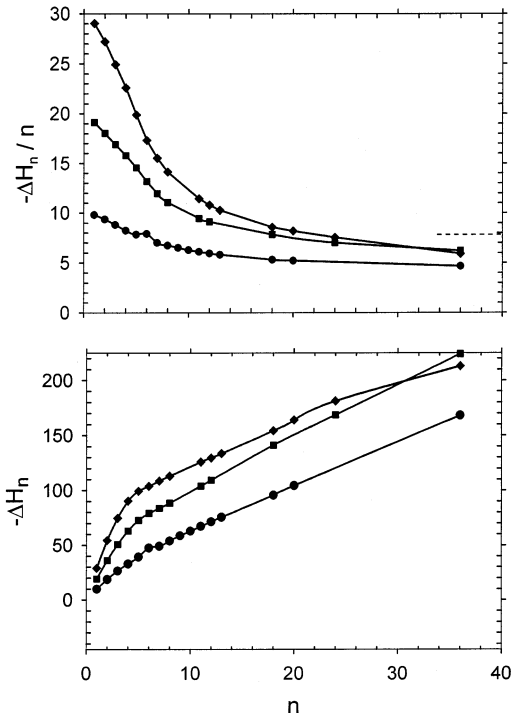

Figure 2. Binding enthalpies ΔH_n from room-temperature Monte Carlo simulations for $Na^+(CH_3CN)_n$ [diamonds], $Cs^+(CH_3CN)_n$ [squares], and $I^-(CH_3CN)_n$ [circles] as a function of cluster size. The top panel displays reduced binding enthalpies $\Delta H_n/n$. The dashed line in the bottom panel is the acetonitrile experimental heat of vaporization.

$I^-(CH_3CN)_{36}$ clusters, respectively. Moreover, the reduced binding enthalpies are smaller than the experimental heat of vaporization at medium cluster size such as $n = 36$. This can be attributed either to the limits of our model potentials or to cluster edge effects. The calculation of the actual heat of vaporization of bulk acetonitrile predicted by our model potentials is left for future work,[93] and it is unclear at this stage whether our model potentials will produce a heat of vaporization in quantitative agreement with experiment. However, cluster edge effects may provide a more likely explanation. On the surface of ionic clusters, there is a deficiency of acetonitrile molecules relative to the bulk liquid situation, which results in less solvation energy for the surface solvent molecules and leads to an underestimation of the reduced binding enthalpy. These findings, as well as the very slow convergence of binding enthalpies to their bulk counterpart with cluster size, are consistent with earlier predictions of the liquid drop model.[94]

Finally, the bottom panel of Figure 2 illustrates the fact that stepwise binding enthalpies (i.e., the slopes of the curves in the bottom panel of Figure 2) decrease with increasing cluster size. As the number of acetonitrile molecules increases, the relative importance of the stronger ion−acetonitrile interactions becomes less significant. Moreover, the decrease observed for smaller ions is faster than that for larger ones, which may reflect the ability of smaller ions to complete solvation shells more rapidly. As a matter of fact, we observe two clearly distinct regimes for cation−acetonitrile clusters that we can actually relate to the cluster structural properties: binding enthalpies first increase very fast up to $n = 6$ for $Na^+(CH_3CN)_n$ and $n = 7$ for $Cs^+(CH_3CN)_n$ clusters, corresponding to strong ion−acetonitrile interactions for the molecules close to the ion; then the binding enthalpy increase seems to slow considerably, because of weaker contributions from solvent molecules further away from the ion. Similar features can be found for $I^-(CH_3CN)_n$ clusters, but they are not as pronounced because of a less well-defined solvation

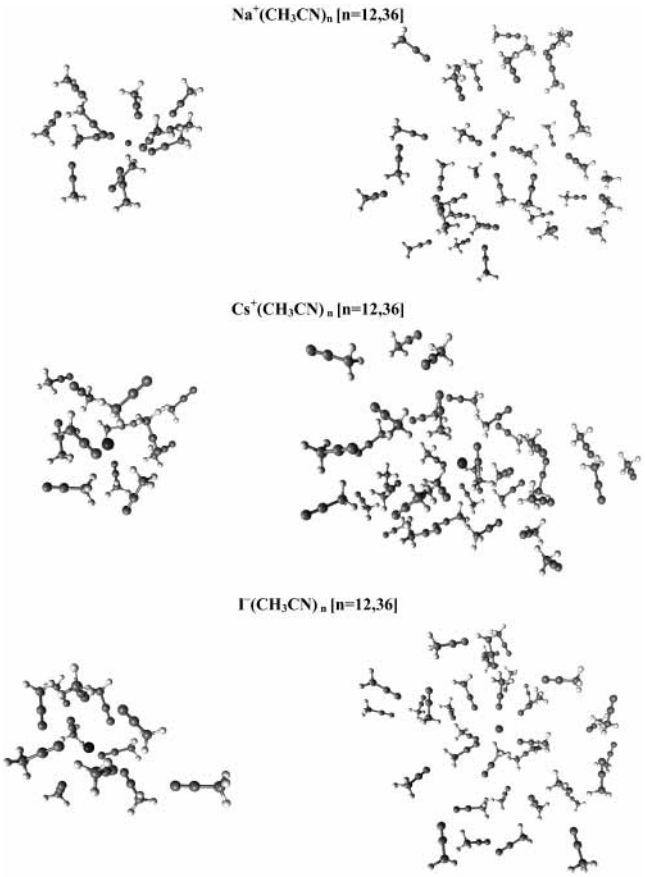

Figure 3. Representative structures of room-temperature $Na^+(CH_3CN)_n$, $Cs^+(CH_3CN)_n$, and $I^-(CH_3CN)_n$ clusters [$n = 12$ and 36] obtained from Monte Carlo simulations employing model potentials.

shell structure. As we shall see shortly, binding enthalpies are closely related to the structure of ionic clusters. Accordingly, we now turn our attention to the structural properties of the clusters.

B. Structural Properties. Figure 3 shows some representative structures of $Na^+(CH_3CN)_n$, $Cs^+(CH_3CN)_n$, and $I^-(CH_3CN)_n$ clusters obtained from room-temperature simulations, for cluster sizes $n = 12$ and 36. The coordination of acetonitrile to ions is naturally via the nitrogen for cations and the methyl hydrogens for iodide, and the corresponding cluster radial probability distributions are shown in Figures 4 and 5. As can be seen immediately from Figure 3, the Na^+, Cs^+, and I^- ions all appear to reside inside the solvent cluster. This interior solvation is a result of the stabilization gained by fully solvating the ion, which seems to overcome the loss of free energy associated with disrupting the solvent structure.[80] In other words, the ion−solvent interactions seem to prevail over solvent−solvent interactions in determining the structure of ionic acetonitrile clusters.

Inspection of Figure 4 reveals that both $Na^+(CH_3CN)_n$ and $Cs^+(CH_3CN)_n$ clusters exhibit a very clear solvation shell structure, identified by sharp, distinct peaks in the probability distributions. The size of the first coordination sphere of $Na^+(CH_3CN)_n$ clusters is ca. 6, which happens to be the same as that computed for the liquid phase with another model potential.[59] We note that, even though the model potentials employed are different,[93] it is not uncommon to find similar coordination numbers for the first solvation shell of ions in both cluster and liquid simulations.[13,17] Since Cs^+ is a larger and more diffuse positive ion than Na^+, the lower binding energy and larger ion−acetonitrile equilibrium distance result in cesium

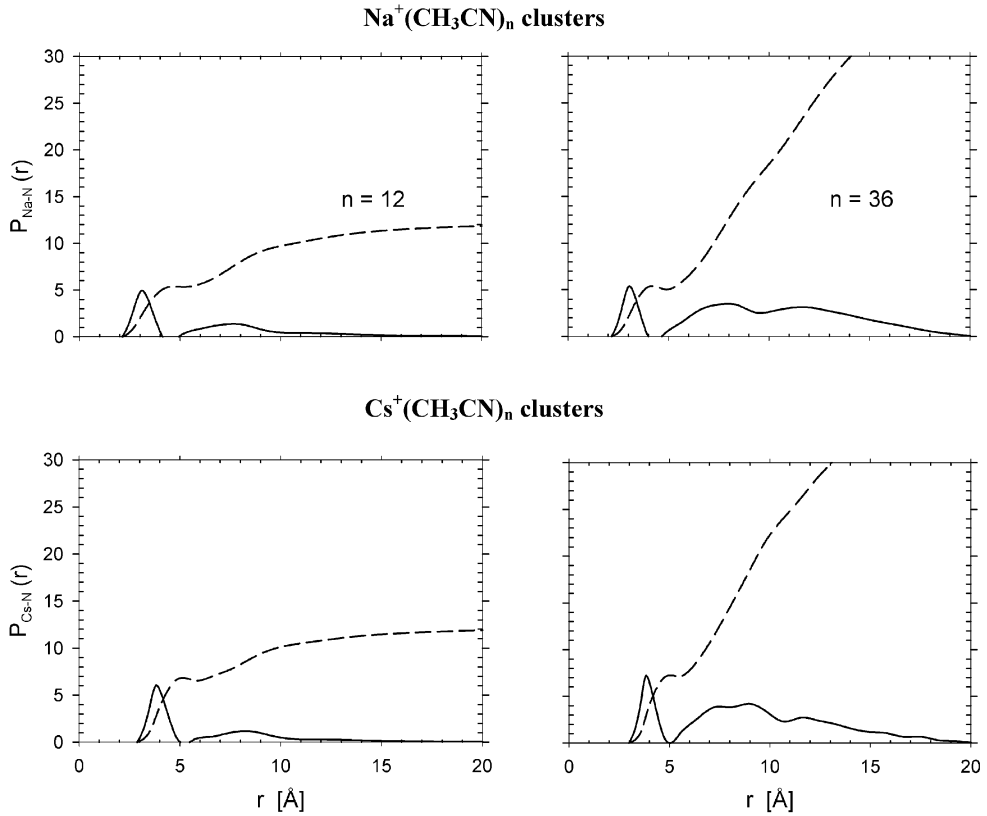

Figure 4. Structural properties of $Na^+(CH_3CN)_n$ [top panel] and $Cs^+(CH_3CN)_n$ [bottom panel] obtained from Monte Carlo simulations. Solid curves are radial probability distribution functions $P(r)$, while dashed curves are the distance-dependent coordination number $N_{coord}(r)$, i.e., the integral of $P(r)$.

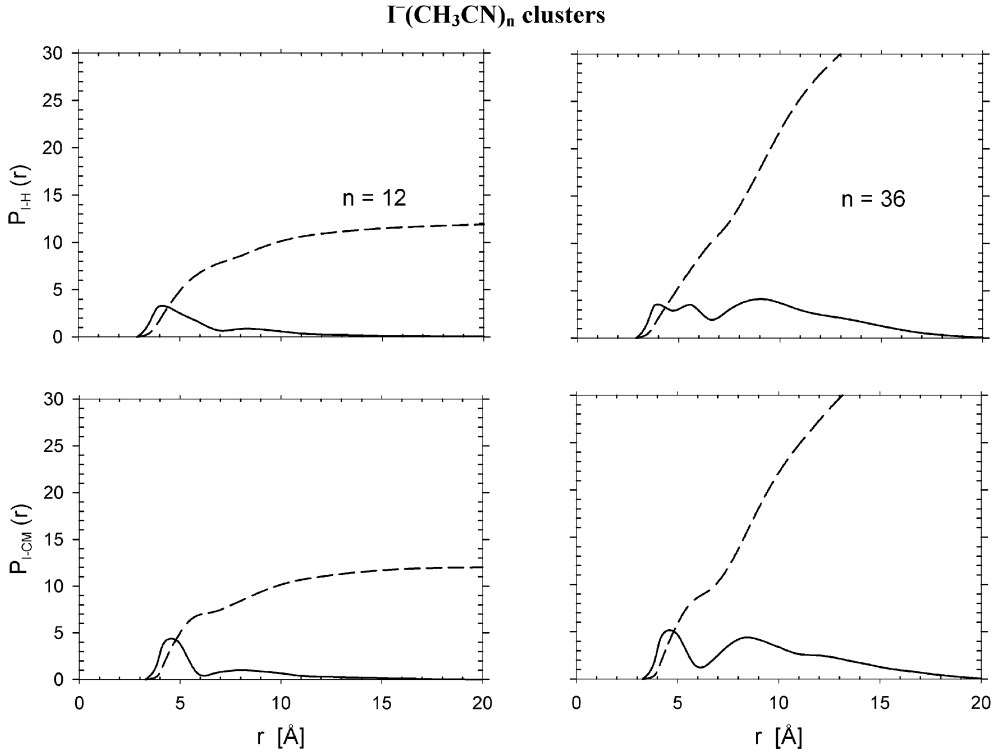

Figure 5. Structural properties of $I^-(CH_3CN)_n$ clusters obtained from Monte Carlo simulations. The top panel shows the ion to hydrogen distance $P_{I-H}(r)$ probability distribution, and the bottom panel the ion to methyl carbon distance $P_{I-CM}(r)$ probability distribution. Solid curves are radial probability distribution functions $P(r)$, while dashed curves are the distance-dependent coordination number $N_{coord}(r)$, i.e., the integral of $P(r)$.

cluster structural properties with broadened peaks in the probability distributions relative to those for sodium clusters. Because of the larger ion−acetonitrile equilibrium distance in $Cs^+(CH_3CN)_n$, solvent steric effects are less significant and the size of the first coordination sphere for $Cs^+(CH_3CN)_n$ clusters increases to 7, compared to that of $Na^+(CH_3CN)_n$ clusters.

In cationic clusters, the high dipole moment of acetonitrile is fully effective toward solvation of the cations via strong

interactions of the metal with the charge concentrated negative nitrogen. On the other hand, because of weaker anion−solvent interactions, via the diffuse charge distribution spread over the hydrogens of acetonitrile, very broad radial probability distributions are observed for $I^-(CH_3CN)_n$ clusters in Figure 5. The spacing between the first two peaks in the ion−hydrogen $P_{H-I}(r)$ probability distributions roughly correspond to the distance between two hydrogens in acetonitrile. Interestingly enough, the solvation shell structure is not immediately evident from the $P_{H-I}(r)$ probability distributions. However, when one plots the ion−methyl carbon $P_{I-CM}(r)$ probability distributions (bottom panel of Figure 5), it becomes evident that $I^-(CH_3CN)_n$ clusters adopt an interior solvation shell structure. The peaks in the $P_{H-I}(r)$ probability distributions in fact correspond to averages over three possible acetonitrile hydrogens interacting with the ion. Whenever one hydrogen is directly coordinated to the ion, the other two are likely to be further away from the ion. As a result of averaging over all hydrogen−iodide distances, multiple peaks appear in the $P_{H-I}(r)$ probability distribution even though the clusters have a clearly defined shell structure. The marked differences observed in the solvation of positive and negative ions are a direct consequence of the nature of the charge distribution of the dipolar solvent molecule. The results for iodide−acetonitrile clusters are also in contrast with results with other solvents such as water, where only one hydrogen per solvent molecule would point toward the ion and the first solvation shell would be represented by a single peak in the ion−hydrogen radial probability distribution. Accordingly, we now turn our attention to a comparison between ion−acetonitrile and ion−water clusters.

C. Comparison with Aqueous Clusters. Inspection of the iodide−acetonitrile cluster radial probability distributions shows that, unlike water, solvent molecules in large acetonitrile clusters are not clearly structured at room temperature. In general, the weak bonding of the solvent molecules and the dipole−dipole nature of the solvent−solvent interactions produce solvent clusters where orientation of any given molecule is correlated only with those of its immediate neighbors, a finding that was observed in high-pressure mass spectroscopy studies of pure clusters.[70,72] On the other hand, it is well-known that the water network is well organized in clusters such as $Na^+(H_2O)_n$ and $I^-(H_2O)_n$ because of relatively strong hydrogen-bonding interactions between water molecules.[25] Another major difference between acetonitrile and water is the solvent molecular size, which causes a significant increase in the ion−molecule distances in clusters and results in much weaker interactions between the ions and more distant solvent molecules, in the second solvation shell for example.

In both $Na^+(CH_3CN)_n$ and $Na^+(H_2O)_n$ clusters, the strong sodium−solvent interactions overcome solvent−solvent interactions, and the ion is thus located inside the solvent cluster. Despite the difference in the solvent molecular size, both $Na^+(CH_3CN)_n$ and $Na^+(H_2O)_n$ clusters have a first solvation shell coordination number of 6.[25] The ion also tends to reside in the interior of the solvent cluster for $I^-(CH_3CN)_n$, in sharp contrast with the situation of $I^-(H_2O)_n$ clusters, where the ion−solvent interactions are not strong enough to allow the ion to disrupt the water network and, consequently, the ion tends to remain at the surface of the cluster up to relatively large cluster sizes.[18,41,95] This feature is very well illustrated by the large ion−solvent center-of-mass (r_{cm}) distances and the nonuniform distributions of the angle θ between solvent molecules, the ion and the solvent center of mass observed for $I^-(H_2O)_n$ clusters.[25,95] Obviously, when the distribution of solvent molecules is not spherically symmetric around the ion, the solvent center of mass is displaced from the ion and the angular distribution differs significantly from a sin θ function.

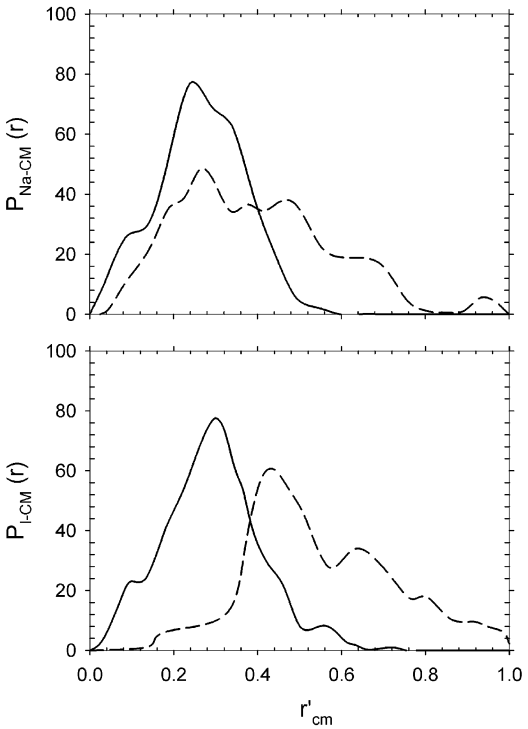

Figure 6. Probability distributions of the scaled ion−solvent center-of-mass distance r'_{cm} (see text) for ion−acetonitrile clusters (solid curve) and ion−water clusters (dashed curve). The top panel displays results for $Na^+(CH_3CN)_n$ and $Na^+(H_2O)_n$, and the bottom panel those for $I^-(CH_3CN)_n$ and $I^-(H_2O)_n$.

Again because of the very different solvent molecular size, ionic clusters of the same size n will have different physical sizes. For example, $Na^+(H_2O)_{20}$ and $I^-(H_2O)_{20}$ clusters have an approximate radius of 5 Å, while their acetonitrile counterparts have a radius of 9 Å. For this reason, and for purpose of comparison between various solvents, we decided to focus on the distributions of ion−solvent center-of-mass distances relative to the cluster radius (r'_{cm}). Shown in Figure 6 are such distributions for sodium and iodide ions in water and acetonitrile clusters. It is immediately evident that $Na^+(CH_3CN)_n$ and $Na^+(H_2O)_n$ clusters have very similar *interior* solvation structures, while those of $I^-(CH_3CN)_n$ and $I^-(H_2O)_n$ clusters differ significantly, i.e., $I^-(CH_3CN)_n$ have interior structures and $I^-(H_2O)_n$ have surface structures. Further support for this fact is provided by the distributions of the angle θ between solvent molecules, the ion and the solvent center of mass shown in Figure 7. While there is a clear deficiency of water molecules on the ion side directly opposite the solvent center of mass, indicative of surface solvation, the angular distribution for acetonitrile clusters is fairly isotropic. This, again, illustrates the importance of the polar nature of the solvent, where strong ion−dipole interactions with acetonitrile ($\mu_{CH_3CN} = 3.92$ D vs $\mu_{H_2O} = 1.85$ D) combined with the absence of strong solvent−solvent interactions (such as hydrogen bonding in water) favor the interior solvation of ions at the expense of disrupting the solvent network.

IV. Concluding Remarks

We have investigated the structural and thermodynamic properties of $Na^+(CH_3CN)_n$, $Cs^+(CH_3CN)_n$, and $I^-(CH_3CN)_n$ clusters by means of room-temperature Monte Carlo simulations.

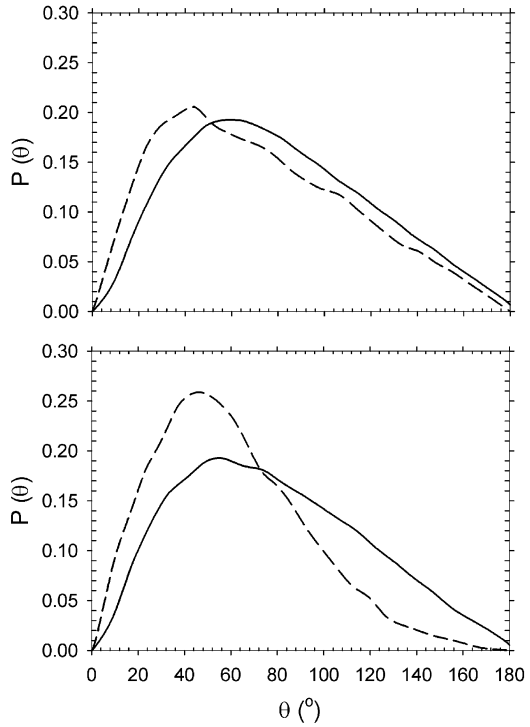

Figure 7. Angular probability distributions for ion−acetonitrile clusters (solid curve) and ion−water clusters (dashed curve). The angle θ is that between an individual solvent molecule, the ion, and the solvent cluster center of mass, as described in ref 25. The top panel displays results for $Na^+(CH_3CN)_n$ and $Na^+(H_2O)_n$, and the bottom panel those for $I^-(CH_3CN)_n$ and $I^-(H_2O)_n$.

An intermolecular model potential has been parameterized that adequately reproduces the small cluster solvent binding energies and structural properties derived from quantum chemistry calculations. One of the remarkable novel features of these model potentials is that they also reproduce the significant increase of the polarity of solvent molecules in the presence of ions (and other solvent molecules) that is observed in quantum chemistry calculations.

The rather successful comparison of the stepwise binding enthalpies obtained from our Monte Carlo simulations with available experimental data suggests that our model potentials are adequate for describing many-body interactions in the clusters. The computed stepwise binding enthalpies for large clusters, which are not accessible experimentally, reach a plateau, slowly converging to the liquid-phase acetonitrile heat of vaporization. The very slow convergence of binding enthalpies to the bulk counterpart with cluster size is consistent with earlier predictions of the liquid drop model.[94] Changes in the evolution of the binding enthalpies of ion−acetonitrile clusters with cluster size seem to reflect the completion of ionic solvation shells, a finding that is less pronounced for iodide−acetonitrile clusters. Binding energies are closely related to the solvation structure of ionic clusters, and differences in the evolution of binding energies with cluster size for anionic and cationic clusters are closely linked to differences in cluster structural properties.

All ion−acetonitrile clusters are found to exhibit an interior solvation structure. Cationic clusters are found to have a very clear solvation shell structure, with sharp peaks in the radial probability distributions. The first solvation shell of $Na^+(CH_3CN)_n$ clusters, like that of $Na^+(H_2O)_n$ clusters, contains six solvent molecules. Weaker ion−solvent interactions cause broadening of the peaks in the radial probability distributions of $Cs^+(CH_3CN)_n$ clusters, accompanied by an increase of the first-shell coordination number to 7. In $I^-(CH_3CN)_n$ clusters, we still observe interior solvation, even though the peaks in the probability distributions appear broader than for cation−acetonitrile clusters, and the coordination number for the first solvation shell equals 9. The interior solvation of $I^-(CH_3CN)_n$ clusters is in sharp contrast to the surface solvation of $I^-(H_2O)_n$ clusters, where the "hydrophobic" iodide tends to sit at the surface of the water network, because ion−solvent interactions are not strong enough to disrupt the stable solvent network. The situation is obviously much different for acetonitrile, and this may result in very different structural and thermodynamic properties of $NaI(CH_3CN)_n$ clusters, which in turn may explain why some aspects of their photodissociation dynamics seem to differ significantly from that of $NaI(H_2O)_n$ clusters.[27]

Acknowledgment. The authors thank Branka M. Ladanyi and James T. Hynes for useful discussions that led to this work. This research was funded by research grants from the Natural Sciences and Engineering Research Council (NSERC) of Canada and the Faculty Research and Development Program (FRDP) of Concordia University. Calculations were performed at the Centre for Research in Molecular Modeling (CERMM), which was established with the financial support of the Concordia University Faculty of Arts & Science, the Ministère de l'Éducation du Québec (MEQ) and the Canada Foundation for Innovation (CFI). T.N.V.N. is the recipient of a Concordia Graduate Fellowship, and G.H.P. holds a Concordia University Research Chair.

References and Notes

(1) Morgan, S.; Keesee, R. G.; Castleman, A. W. *J. Am. Chem. Soc.* **1989**, *111*, 3841.
(2) Markovich, G.; Pollack, S.; Giniger, R.; Cheshnovsky, O. *J. Chem. Phys.* **1994**, *101*, 9344.
(3) Abraham, M. H. *Prog. Phys. Org. Chem.* **1974**, *11*, 1.
(4) Parker, A. J. *Chem. Rev.* **1969**, *1*, 69.
(5) Marchi, M.; Sprik, M.; Klein, M. L. *Faraday Discuss. Chem. Soc.* **1988**, *85*, 373.
(6) Tzeng, W. B.; Wei, S.; Castleman, A. W. *J. Am. Chem. Soc.* **1989**, *111*, 6035.
(7) Batista, V. S.; Coker, D. F. *J. Chem. Phys.* **1997**, *106*, 7102.
(8) Snyder, E. M.; Castleman, A. W. *J. Chem. Phys.* **1997**, *107*, 744.
(9) Syage, J. A.; Steadman, J. *J. Phys. Chem.* **1992**, *96*, 9606.
(10) Radlof, W.; Freudenberg, T.; Stert, V.; Ritze, H.-H.; Noack, F.; Hertel, I. V. *Chem. Phys. Lett.* **1997**, *264*, 210.
(11) Bernstein, E. R. *Chemical Reactions in Clusters*; Oxford University Press: New York, 1996.
(12) Gough, T. *Atomic and Molecular Beam Methods*; Scoles, G., Lainé, D., Valbusa, U., Eds.; Oxford University Press: Oxford, 1992; Vol. 2.
(13) Jorgensen, W. L.; Bigot, B.; Chandrasekhar, J. *J. Am. Chem. Soc.* **1981**, *104*, 4584.
(14) Markovich, G.; Perera, L.; Berkowitz, M. L.; Cheshnovsky, O. *J. Chem. Phys.* **1996**, *105*, 2675.
(15) Hirao, K.; Yamabe, S.; Sano, M. *J. Chem. Phys.* **1982**, *86*, 2626.
(16) Draves, J. A.; Luthey-Schulten, Z.; Liu, W.-L.; Lisy, J. M. *J. Chem. Phys.* **1990**, *93*, 4589.
(17) Selegue, T. J.; Moe, N.; Draves, J. A.; Lisy, J. M. *J. Chem. Phys.* **1992**, *96*, 7268.
(18) Serxner, D.; Dessent, C. E. H.; Johnson, M. A. *J. Chem. Phys.* **1996**, *105*, 7231. Ayotte, P.; Bailey, C. G.; Weddle, G. H.; Johnson, M. A. *J. Phys. Chem. A* **1998**, *102*, 3067.
(19) Ayala, R.; Martinez, J. M.; Pappalardo, R. R.; Marcos, E. S. *J. Phys. Chem. A* **2000**, *104*, 2799.
(20) Okuno, Y. *J. Phys. Chem. A* **1999**, *103*, 190.
(21) Asada, T.; Nishimoto, K. *Chem. Phys. Lett.* **1995**, *232*, 518.
(22) Gertner, B. J.; Peslherbe, G. H.; Hynes, J. T. *Isr. J. Chem.* **2000**, *40*, 273.
(23) Kusada, I.; Wang, Z.-G.; Seinfeld, J. H. *J. Chem. Phys.* **1998**, *108*, 6829.
(24) Kim, S. K.; Breen, J. J.; Willberg, D. M.; Peng, L. W.; Heikal, A.; Syage, J. A.; Zewail, A. *J. Phys. Chem.* **1995**, *99*, 7421.
(25) Peslherbe, G. H.; Ladanyi, B. M.; Hynes, J. T. *Chem. Phys.* **2000**, *258*, 201.

(26) Peslherbe, G. H.; Ladanyi, B. M.; Hynes, J. T. *J. Phys. Chem. A* **2000**, *104*, 4533.
(27) Grégoire, G.; Mons, M.; Dedonder-Lardeux, C.; Jouvet, C. *Eur. Phys. J. D* **1998**, *1*, 5.
(28) Grégoire, G.; Mons, M.; Dimicoli, I.; Dedonder-Lardeux, C.; Jouvet, C.; Martrenchard, S.; Soldagi, D. *J. Chem. Phys.* **1999**, *110*, 1521.
(29) Grégoire, G.; Mons, M.; Dimicoli, I.; Dedonder-Lardeux, C.; Jouvet, C.; Martrenchard, S.; Soldagi, D. *J. Chem. Phys.* **2000**, *112*, 8794.
(30) Dedonder-Lardeux, C.; Grégoire, G.; Jouvet, C.; Martrenchard, S.; Solgadi, D. *Chem. Rev.* **2000**, *100*, 4023.
(31) Wang, W.; Low, P. J.; Carty, A. J.; Sappa, E.; Gervasio, G.; Mealli, C.; Ienco, A.; Perez-Carreno, E. *Inorg. Chem.* **2000**, *39*, 998.
(32) Jungwirth, P. *J. Phys. Chem. A* **2000**, *104*, 145.
(33) Re, S.; Osamura, Y.; Morokuma, K. *J. Phys. Chem. A* **1999**, *103*, 3535.
(34) Jensen, F. *Introduction to Computational Chemistry*; Wiley: West Sussex, England, 1999.
(35) Engel, V.; Metiu, H. *J. Chem. Phys.* **1989**, *90*, 6116.
(36) Braun, M.; Meier, C.; Engel, V. *J. Chem. Phys.* **1996**, *105*, 530.
(37) Martinez, T. J.; Levine, R. D. *Chem. Phys. Lett.* **1996**, *259*, 252.
(38) Rosker, M. J.; Rose, T. S.; Zewail, A. H. *Chem. Phys. Lett.* **1988**, *146*, 175. Rose, T. S.; Rosker, M. J.; Zewail, A. H. *J. Chem. Phys.* **1988**, *88*, 6672. Rose, T. S.; Rosker, M. J.; Zewail, A. H. *J. Chem. Phys.* **1989**, *91*, 7415. Cong, P.; Mohktari, A.; Zewail, A. H. *Chem. Phys. Lett.* **1990**, *172*, 109. Mohktari, A.; Cong, P.; Herek, J. L.; Zewail, A. H. *Nature* **1990**, *348*, 225. Cong, P.; Roberts, G.; Herek, J. L.; Mohktari, A.; Zewail, A. H. *J. Chem. Phys.* **1996**, *100*, 7832.
(39) Jouvet, C.; Martrenchard, S.; Solgadi, D.; Dedonder-Lardeux, C.; Mons, M.; Grégoire, G.; Dimicoli, I.; Piuzzi, F.; Visticot, J. P.; Mestdagh, J. M.; Doliveira, P.; Meynadier, P.; Perdrix, M. *J. Phys. Chem.* **1997**, *101*, 2555.
(40) Peslherbe, G. H.; Ladanyi, B. M.; Hynes, J. T. *J. Phys. Chem.* **1998**, *102*, 4100.
(41) Perera, L.; Berkowitz, M. L. *J. Chem. Phys.* **1991**, *95*, 1954, 4236. Perera, L.; Berkowitz, M. L. *J. Chem. Phys.* **1993**, *99*, 4236. Perera, L.; Berkowitz, M. L. *J. Chem. Phys.* **1993**, *99*, 4222. Dang, L. X.; Garrett, B. C. *J. Chem. Phys.* **1993**, *99*, 2972. Dang, L. X.; Smith, D. E. *J. Chem. Phys.* **1993**, *99*, 6950.
(42) Harpham, M.; Ladanyi, B. M.; Hynes, J. T.; Peslherbe, G. H., manuscript in preparation.
(43) Edwards, H. J.; Madden, P. A.; McDonald, I. R. *Mol. Phys.* **1984**, *51*, 1141.
(44) Jorgensen, W. L.; Briggs, J. M. *Mol. Phys.* **1988**, *61*, 3845.
(45) Bohm, H. J.; McDonald, I. R.; Madden, P. A. *Mol. Phys.* **1983**, *49*, 347.
(46) Cabaleiro-Lago, E. M.; Rios, M. A. *J. Phys. Chem. A* **1997**, *101*, 8327.
(47) Jouvet, C., personal communication.
(48) Hiraoka, K.; Mizuse, S. *J. Phys. Chem.* **1988**, *92*, 3943.
(49) Metropolis, N.; Rosenbluth, A. W.; Rosenbluth, M. N.; Teller, A. H.; Teller, E. *Simulations of Liquids and Solids*; Ciccotti, G., Frenkel, D., McDonald, I. R., Eds.; North-Holland: New York, 1987.
(50) Press, W. H.; Teulkolsky, S. A.; Vetterling, W. T.; Flannery, B. P. *Numerical Recipes, The Art of Scientific Computing*; Cambridge University Press: Cambridge, 1992.
(51) Allen, M. P.; Tildesley, D. J. *Computer Simulations of Liquids*; Oxford University Press: New York, 1989.
(52) Asher, R. L.; Micha, D. A.; Brucat, P. J. *J. Chem. Phys.* **1992**, *96*, 7683.
(53) The boiling point of liquid acetonitrile is 81.6 °C.
(54) Cabarcos, O. M.; Lisy, J. M. *Chem. Phys. Lett.* **1996**, *257*, 265.
(55) Lu, D. S.; Singer, S. J. *J. Chem. Phys.* **1995**, *103*, 1913.
(56) Lu, D. S.; Singer, S. J. *J. Chem. Phys.* **1996**, *105*, 3700.
(57) Rappé, A. K.; Casewit, C. J. *Molecular Mechanics across Chemistry*; University Science Books: Sausalito, California, 1997; p 407.
(58) The distributed polarizability model of ref 14 fails to reproduce the solvent induced dipole moments predicted by ab initio calculations for small ion−acetonitrile clusters.
(59) Cabaleiro-Lago, E. M.; Rios, M. A. *Chem. Phys.* **1998**, *236*, 235.
(60) Dang, L. X.; Chang, T. M. *J. Chem. Phys.* **1997**, *106*, 8149.
(61) Perera, L.; Amar, F. G. *J. Chem. Phys.* **1989**, *90*, 8274.
(62) Schmidt, M. W.; Balridge, K. K.; Boatz, J. A.; Elbert, S. T.; Gordon, M. S.; Jensen, J. H.; Matsunaga, N.; Nguyen, K. A.; Su, S. J.; Windus, T. L.; Dupuis, M.; Montgomery, J. A. *J. Comput. Chem.* **1993**, *14*, 1347.
(63) Frisch, M. J.; Trucks, G. W.; Schlegel, H. B.; Scuseria, G. E.; Robb, M. A.; Cheeseman, J. R.; Zakrzewski, V. G.; Jr., J. A. M.; Stratmann, R. E.; Burant, J. C.; Dapprich, S.; Millam, J. M.; Daniels, A. D.; Kudin, K. N.; Strain, M. C.; Farkas, O.; Tomasi, J.; Barone, V.; Cossi, M.; Cammi, R.; Mennucci, B.; Pomelli, C.; Adamo, C.; Clifford, S.; Ochterski, J.; Petersson, G. A.; Ayala, P. Y.; Cui, Q.; Morokuma, K.; Malick, D. K.; Rabuck, A. D.; Raghavachari, K.; Foresman, J. B.; Cioslowski, J.; Ortiz, J. V.; Stefanov, B. B.; Liu, G.; Liashenko, A.; Piskorz, P.; Komaromi, I.; Gomperts, R.; Martin, R. L.; Fox, D. J.; Keith, T.; Al-Laham, M. A.; Peng, C. Y.; Nanayakkara, A.; Gonzalez, C.; Challacombe, M.; Gill, P. M. W.; Johnson, B.; Chen, W.; Wong, M. W.; Andres, J. L.; Gonzalez, C.; Head-Gordon, M.; Replogle, E. S.; Pople, J. A. *Gaussian 98*, Rev. A7, Gaussian Inc.: Pittsburgh.
(64) Hehre, W. J.; Radom, L.; Schleyer, P. v. R.; Pople, J. A. *Ab Initio Molecular Orbital Theory*; John Wiley and Sons: New York, 1985.
(65) Levine, I. N. *Quantum chemistry*; Prentice Hall Inc.: Englewood Cliffs, New Jersey, 1991.
(66) Becke, A. D. *J. Chem. Phys.* **1993**, *98*, 5648.
(67) Bergner, A.; Dolg, M.; Kuchle, W.; Stoll, H.; Preuss, H. *Mol. Phys.* **1993**, *80*, 1431.
(68) Glukhovtsev, M. N.; Pross, A. *J. Chem. Phys.* **1995**, *103*, 1878.
(69) Bases of 6-311+G(2df) quality have not been reported for iodide and cesium. We augmented the iodide 6-311+G(df) and cesium/iodide SDD bases accordingly with diffuse and/or polarization functions with optimized exponents.
(70) Bertagnolli, H.; Chieux, P.; Zeidler, M. D. *Mol. Phys.* **1976**, *32*, 759.
(71) Costain. *J. Chem. Phys.* **1958**, *29*, 864.
(72) Steiner, P. A.; Gordy, W. *J. Mol. Spectrosc.* **1966**, *21*, 291.
(73) Singh, U. C.; Kollman, P. A. *J. Comput. Chem.* **1984**, *5*, 129.
(74) Boys, S. F.; Bernardi, F. *Mol. Phys.* **1970**, *19*, 553.
(75) Chalasinski, G.; Szczesniak, M. *Chem. Rev.* **1994**, *94*, 1723.
(76) VanDuijneveldt, F. B.; VanDuijneveldt-VanDeRijdt, J. G. C. M.; VanLenthle, J. H. *Chem. Rev.* **1994**, *94*, 1873.
(77) Reimers, J. R.; Hall, L. E. *J. Am. Chem. Soc.* **1999**, *121*, 3730.
(78) Popelier, P. L. A.; Stone, A. J.; Wales, D. J. *Faraday Discuss.* **1994**, *97*, 243.
(79) Dessent, C. E. H.; Kim, J.; Johnson, M. A. *J. Phys. Chem.* **1996**, *100*, 12.
(80) Radnai, T.; Itoh, S.; Ohtaki, H. *Bull. Chem. Soc.* **1988**, *61*, 3845.
(81) Davidson, W. R.; Kebarle, P. *J. Am. Chem. Soc.* **1976**, *98*, 6125.
(82) Glendening, E. D.; Feller, D. *J. Phys. Chem.* **1995**, *99*, 3060.
(83) Timerghazin, Q. K.; Peslherbe, G. H. *Chem. Phys. Lett.* **2002**, *354*, 31.
(84) Timerghazin, Q. K.; Nguyen, T. N.; Peslherbe, G. H. *J. Chem. Phys.* **2002**, *116*, 6867.
(85) Timerghazin, Q. K.; Peslherbe, G. H., work in progress.
(86) Nguyen, T. N.; Timerghazin, Q. K.; Peslherbe, G. H. *J. Phys. Chem.*, submitted.
(87) Besler, B. H.; Merz, K. M., Jr.; Kollman, P. A. *J. Comput. Chem.* **1990**, *11*, 431.
(88) Tessman, J. R.; Kahn, A. H. *Phys. Rev.* **1953**, *92*, 890.
(89) Lide, D. R. *The CRC Handbook of Chemistry and Physics*, 75th ed.; CRC Press: Boca Raton, Florida, 1994.
(90) The σ_{ij} size parameters were expressed via the usual Lorentz−Berthelot combination rule as a function of atomic σ_i and σ_j, which we tried to keep proportional to the atomic and/or ionic van der Waals radii of the particles during the fitting procedure. However, we found it necessary to derive each ϵ_{ij} parameter independently, without any actual physical constraint.
(91) We note that the MP2 level of theory seems to systematically underestimate the cluster binding energies, compared to the higher level CCSD(T). Thus, for the larger clusters where no CCSD(T) data is available, we preferentially choose model parameters that tend to predict model binding energies that are larger than their MP2 counterparts.
(92) Putnam, W. E.; McEachern, D. M.; Kilpatrick, J. E. *J. Chem. Phys.* **1965**, *42*, 749.
(93) Liquid simulations with our model potentials are under way for a consistent comparison of cluster and liquid results. Nguyen, T. N.; Peslherbe, G. H., work in progress.
(94) Peslherbe, G. H.; Ladanyi, B. M.; Hynes, J. T. *J. Phys. Chem. A* **1999**, *103*, 2561.
(95) Koch, D. M.; Peslherbe, G. H. *Chem. Phys. Lett.* **2002**, in press.
(96) Quina, F. H.; Politi, M. J.; Cuccovia, J. M.; Baumgarten, E.; Martins-Franchetti, S. M.; Chaimovich, H. *J. Phys. Chem.* **1980**, *84*, 361.
(97) Hiraoka, K.; Takimoto, H.; Yamabe, S. *J. Phys. Chem.* **1986**, *90*, 5910.